



Article

Method for Benchmarking Li Metal Anodes: A Mandatory Step toward Reliable Lithium Metal Batteries

Nicolas Delaporte *, Alexis Perea, Mireille Léonard, Julie Matton, Hendrix Demers , Steve Collin-Martin, David Rozon, Daniel Clément, Abdelbast Guerfi and Chisu Kim

Center of Excellence in Transportation, Electrification and Energy Storage, 1806 Bd. Lionel-Boulet, Varennes, QC J3X 1S1, Canada; perea.alexis2@hydroquebec.com (A.P.); leonard.mireille@hydroquebec.com (M.L.); matton.julie@hydroquebec.com (J.M.); demers.hendrix@hydroquebec.com (H.D.); collin-martin.steve2@hydroquebec.com (S.C.-M.); rozon.david@hydroquebec.com (D.R.); clement.daniel@hydroquebec.com (D.C.); guerfi.abdelbast@hydroquebec.com (A.G.); kim.chisu@hydroquebec.com (C.K.)

* Correspondence: delaporte.nicolas@hydroquebec.com

Abstract: All-solid-state batteries are known to be the new energy storage holy grail that will lead to safer batteries with higher energy density than current Li-ion batteries. The use of a solid electrolyte enables the use of lithium metal as the anode material. However, its composition, its thickness, and the quality/nature of its passivation layer can strongly affect the performance of the battery. For this reason, we propose a simple benchmarking method that evaluates and compares the quality and electrochemical performance of various Li anodes. This method can be easily reproduced, especially concerning the electrochemical evaluation that uses a commercial liquid electrolyte and the widely spread coin-cell format. In total, ~285 coin cells were assembled to benchmark our in-house lithium metal foil (Lithium HQ) with two commercial ones and the results showed the superior performance of our Li metal anode. The performance of the cells seems closely related to the quality and uniformity of the Li surface. In addition, we propose including in the benchmarking method the effect of Li aging in a dry room on the electrochemical performance. This effect is important to consider because the fabrication of all-solid-state batteries is conducted in such an environment.



Citation: Delaporte, N.; Perea, A.; Léonard, M.; Matton, J.; Demers, H.; Collin-Martin, S.; Rozon, D.; Clément, D.; Guerfi, A.; Kim, C. Method for Benchmarking Li Metal Anodes: A Mandatory Step toward Reliable Lithium Metal Batteries. *Batteries* **2023**, *9*, 368. <https://doi.org/10.3390/batteries9070368>

Academic Editor: Federico Baronti

Received: 8 May 2023

Revised: 3 June 2023

Accepted: 6 July 2023

Published: 8 July 2023



Copyright: © 2023 by the authors. Licensee MDPI, Basel, Switzerland. This article is an open access article distributed under the terms and conditions of the Creative Commons Attribution (CC BY) license (<https://creativecommons.org/licenses/by/4.0/>).

1. Introduction

- A benchmarking method to evaluate Li anodes performance was proposed.
- In total, 285 coin-cells were assembled to compare three Li anodes.
- Physical characterizations revealed the better surface quality of the in-house Li.
- The cells performance is related to the quality and uniformity of the Li surface.

The aging of Li anodes in a dry room for three weeks was evaluated.

In 2050, according to the International Energy Agency's Net Zero by 2050 report [1], the global transportation sector must reach a net-zero emissions target, which implies 100% electric vehicle sales by 2035. Presently, electric vehicles are equipped with Li-ion batteries, which largely dominate the market due to their high energy densities and long lifespan. However, safety concerns are already a problem that must be seriously addressed in light of the ambitious plans for transportation electrification [2]. Worldwide studies for developing safer batteries are ongoing and a new kind of electrochemical system, called all solid-state batteries (ASSB), is believed to be a game changer for the future [3]. Instead of flammable organic solvents, a solid electrolyte is used that improves the security of the battery as well as the energy density. This solid electrolyte acts as a physical barrier for lithium dendrites and thus enables the use of Li metal anode. It had fallen into disuse for decades because of its ability to form dendrites that could lead to internal short circuits [4], but now, due to the increasing demand for energy, there has been a rush for Li metal again. Thanks to its high

theoretical specific capacity ($3860 \text{ mAh}\cdot\text{g}^{-1}$) and its low redox potential (-3.04 V vs. standard hydrogen electrode), Li metal is paving the way for high energy density batteries [5].

In recent years, enormous efforts have been made in the field of characterization technologies, theoretical calculation methods, and *in situ* experiments to understand the failure mechanism of lithium metal. On the other hand, the high reactivity of lithium metal to contamination, its purity, and its morphology as an anode evoke an important subject to be addressed. It is undeniable that the manufacturing method of the lithium anode has a direct relationship to these parameters, and the impact will be reflected in the performance of the cell. However, it must be expected that lithium metal will have extreme reactivity when operated or handled under normal conditions. If exposed to air, even at room temperature, it reacts with traces of H_2O , oxygen, nitrogen, carbon dioxide in the air forming Li_2CO_3 , Li_2O , LiOH , and possibly also Li_3N on the surface [6]. It is therefore very difficult to obtain metallic lithium with a very clean surface. These typical contaminants for Li will be major challenges for all approaches to its production, in addition to thickness variation.

Several approaches have recently been developed to meet the challenge of thin lithium anode production. One such approach is the electrodeposition of thin layers of lithium metal using electrolytic baths [7]. Indeed, this approach required simple equipment with roll-to-roll (R2R), but these are slow processes, and they also involve significant costs for the recycling of the electrolyte, factors which strongly affect profitability. Physical vapor deposition (PVD) is another approach; it enables the production of a superior quality of thin layers of Li using R2R [8]. The disadvantage of this approach, however, is that it incurs high costs associated with equipment requiring a high vacuum and with operation and maintenance. The other common process is traditional extrusion and rolling for metals such as steel or aluminum, using the cohesive force of these to achieve the desired flatness and thickness. At the same time, for the manipulation of the Li^0 , it is obvious that the Li^0 cannot be subjected to such physical constraints [9]. To achieve the desired thickness, roller pressure and speed can be optimized. Despite its ease and the R2R process, grain boundaries are inevitably formed on the surface which can be dendrite nucleation points due to the irregularity of the surface current. Therefore, each lithium anode produced has a typical characteristic, depending on the approach used.

On the other hand, we know that the practical SEI layer is fragile and shape-sensitive, so if the Li surface morphology is not uniform or not properly clean, it will lead to unevenly distributed current density on the surface, which could initiate the formation of dendritic lithium. However, the SEI layer on lithium metal is extremely critical: it is the bottleneck of the lithium anode because its stability leads to a positive impact on the transport properties and the homogeneity of the electrodeposited/dissolved Li film during charging/discharging. Consequently, any approach always has advantages and disadvantages, whether technical or cost-related.

Until now, especially for the Li anode, no “standard method” is accessible and used by researchers working on the development of Li metal and solid-state batteries to evaluate and compare various sources of battery materials. It is widely accepted that fabrication methods [7,10,11], size a Li grains [12], thickness of Li anodes [13] or nature of the natural/artificial passivation layers could impact the electrochemical performance in batteries as well as the Li metal stability upon storage. However, comparisons with other research works when publishing a scientific paper is mandatory, but, due to the absence of standardized method as well as the utilization of a large variety of “electrochemical platforms” and different sources of battery materials, comparisons are often unfruitful and not representative of reality. With the growing enthusiasm for Li metal and all-solid-state batteries, a benchmarking method to compare different sources of lithium must be designed rapidly.

In this paper, we propose a simple method for evaluating and comparing the quality and electrochemical performance of different lithium anode sources. Two commercial lithium foils, named Lithium #1 and Lithium #2, were compared with our internal lithium metal foil (Lithium HQ). The method was designed to be easily replicated by other research groups, particularly the electrochemical test part. In fact, the symmetrical Li/Li cells are assembled

using a commercial liquid electrolyte and in the coin format most widely used for material validation or comparison. In total, ~285 coin cells were assembled with the three Li foils, and the results showed the superior performance of our Li metal anode, which revealed the better surface quality of HQ Lithium compared with commercial Li foils. It could be established that cell performance is linked to the quality and uniformity of the Li surface.

2. Experimental Section

2.1. Method Proposed for Benchmarking Li Metal Anodes

The method proposed is firstly designed to compare the quality of the lithium foil in terms of surface contaminations, roughness, and hardness, as well as distribution of Li grains. Secondly, and most importantly, electrochemical performance is assessed with a simple method, easily repeatable by other research groups or universities. Basically, coin cells have been selected due to their wide utilization in this research domain in comparison with pouch-cells, for instance, which require more devices and knowledge. To facilitate comparison of results with other studies, we used a commercial carbonate-based electrolyte that is widely used. Thirdly and optionally, the method proposes comparing the aging of Li foils in a dry room for several days. In this study, a period of 3 weeks was considered as a first screening, but it could be longer to reveal more differences between various Li anodes. Scheme 1 presents the general procedure of the experimental setup. Lithium HQ was produced by an extrusion and rolling method. Firstly, an ingot of the lithium metal was transformed into lithium foil of 250 μm thickness using an extruder. Then, the thickness of the lithium foil was further reduced to 45 μm by laminating the lithium foil between the rolls. An in-house designed rolling machine was used inside a dry room having a dew point of less than -45°C . Lithium HQ fabricated by Hydro-Québec is compared with two commercial lithium foils (Lithium #1 and #2) having a similar thickness. At their reception, they are immediately stored in a glove box under Ar ($\text{O}_2 < 0.5 \text{ ppm}$, $\text{H}_2\text{O} < 0.5 \text{ ppm}$) to avoid exposure to air. Generally, Li foils are initially packed and shipped within a controlled and inert atmosphere. The different lithium foils are cut with dimensions of approximately 20 cm \times 8 cm (enough to make several coin cells and samples for various characterization). Pre-dried metal plastic bags are used to individually store Li metal strips. A sheet for each lithium, sealed in its metal plastic bag, is kept inside the glove box without exposure to the atmosphere of the dry room; this sample is coded “ t_0 ” (0 h exposure). Other pieces of Li foils are suspended from one side to expose their entire surface to the dry room atmosphere. The photograph for Scheme 1 shows the experiment set up with the dew point probe at the bottom of the samples for closely monitoring the humidity level. Figure 1a shows the dew point data recorded for 500 h (~3 weeks). The dew point fluctuated between -56°C and -65°C , confirming the low humidity level in the dry room atmosphere. An equation (Equation (1)) can be generated from the curve that plots the relative humidity as a function of dew point at 21°C (temperature inside the dry room, see Figure S1 in Supplementary Materials):

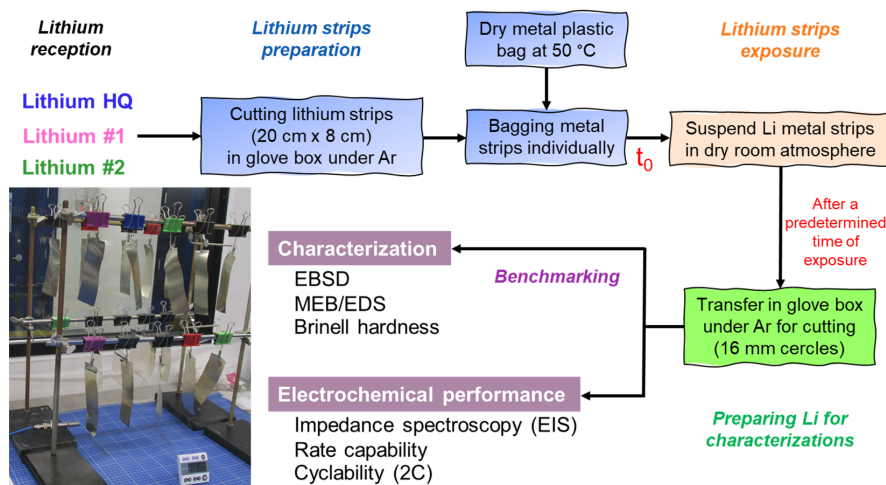
$$y = 73.501e^{(0.1148x)} \quad (1)$$

Thus, the relative humidity varied mainly between 0.05 to 0.1%. After different exposure times (i.e., 1 h, 5 h, 24 h, 48 h, 72 h, 1 week, 2 and 3 weeks), the lithium foil is detached and transferred inside the glove box under argon to be cut into 16-mm-diameter disk pieces for cell assembly and characterization.

2.2. Characterizations

The morphology and the elemental composition analysis of the Li surface were analyzed using an SU-7000 SEM by Hitachi and a windowless energy dispersive spectrometer (EDS) Ultim Extreme by Oxford Instruments. This EDS detects the Li K α X-ray from metallic lithium [14]. The micrograph and X-ray maps were acquired at an accelerating voltage of 5 kV to allow the detection of the Li K α X-ray signal, a probe current of 3.6 nA, and a working distance of 6 mm. Acquisition times of 1 min and 5 min were used for the X-ray spectrum and the maps, respectively. The X-ray intensities were extracted from the spectrum using the

AZtec (version 5.0 SP1) by Oxford Instruments. The intensities were normalized using the f-ratio method [15]. This method eliminates the effect of current variation between acquisition and the values are proportional to the element concentration, which allows one to compare the composition for different lithium samples. For each sample, five measures have been made and the mean and standard deviation are calculated and plotted.



Scheme 1. Schematic representation of the method proposed for benchmarking of Li anodes. After the Li foils are received, Li strips are prepared within an inert atmosphere and individually sealed in pre-dried metal plastic bags. The Li sheets are then suspended in the dry room atmosphere for a predetermined exposure time. After this exposure, they are transferred to a glove box under argon to be cut into circles 16 mm in diameter for characterizations. The experimental setup is represented by the photograph on the left side of the scheme.

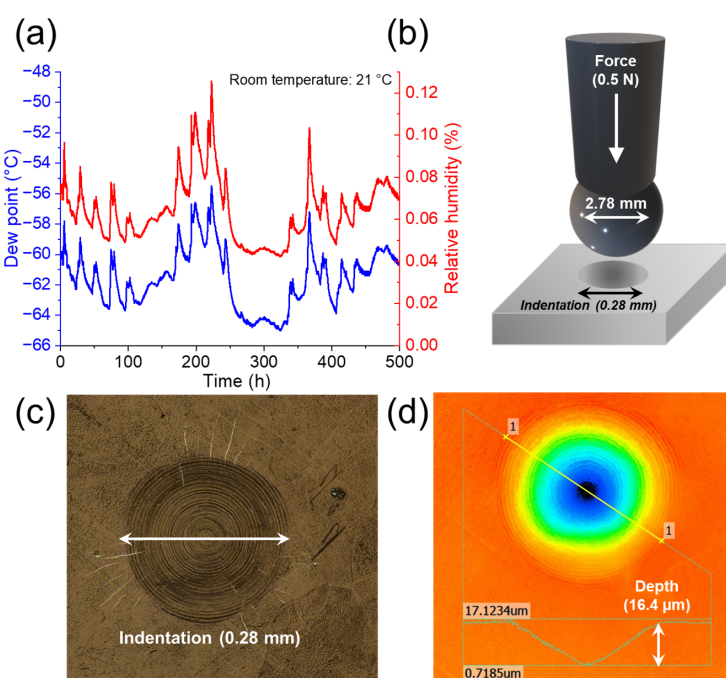


Figure 1. (a) Evolution of dew point (blue line) and relative humidity (red line) close to the setup at constant room temperature of 21 °C. Data recorded with a calibrated dew point probe during the entire experiment (~500 h). (b) Schematic representation of the spherical indenter tip used to apply a permanent deformation on the Li surface; (c) Optical image; and (d) Laser scanning confocal image (height view) of a typical indentation mark after applying a force of 0.5 N on the Li surface for 30 s. The depth profile gives a depth of approximately 16.4 μ m for a diameter of 0.28 mm.

Crystallographic information was obtained using electron backscatter diffraction (EBSD) with a Symmetry detector by Oxford Instruments on an SEM SU-7000 by Hitachi. The sample surfaces were prepared using in-plane ion milling with an IM5000 ArBlade by Hitachi in 2 milling steps. In the first step, an intermittent Ar beam (30 s on and 90 s off) of 6 kV was used for a 10 min milling and the sample was rotated at 25 RPM at an angle of 85°. In the second step, the accelerating voltage was decreased to 3 kV for a 15 min milling. The EBSD maps were acquired at an accelerating voltage of 20 kV, a probe current of 7.6 nA, and a working distance of 15 mm. The EBSD maps were analyzed with HKL Channel 5 software by Oxford Instruments. Noise reduction (data cleaning) was applied to the EBSD map to reduce the number of zero solutions and wild spikes.

The indentation marks on the Li surface are obtained with a DMA 850 TA instrument equipped with a spherical indenter tip 2.78 mm in diameter. A constant force of 1×10^{-5} or 0.5 N is applied on the metal surface for 30 s. Nine measures are performed for each lithium sample and the mean and standard deviation are calculated and plotted.

Optical and 3D laser scanning confocal images of various indentation marks on the lithium surface are obtained with a Keyence VK-x200 3D laser microscope at 50× magnification. The diameter and depth of the indentation marks are calculated using VK analyzer software. The Brinell hardness number (BHN) is calculated with the following equation (Equation (2)):

$$BHN = \frac{2F}{\pi D(D - \sqrt{D^2 - d^2})} \quad (2)$$

where F = applied force (N), D = diameter of indenter tip (mm), d = diameter of indentation mark (mm).

Figure 1 shows; (b) a schematic representation of the spherical indenter tip used to apply the permanent deformation on the Li surface, as well as (c) an optical image and (d) a 3D confocal laser scanning image of an indentation mark to easily calculate its diameter and then the Brinell hardness.

2.3. Assembly of Coin Cells and Electrochemical Characterization

The in-house lithium metal produced by Hydro-Québec (Shawinigan, QC, Canada), and the two commercial ones (denoted Lithium #1 and Lithium #2), have a thickness of about 45–50 µm. Pieces of lithium in the shape of discs 16 mm in diameter after exposure for different times as well as the sample of lithium “ t_0 ” are assembled in CR2032 type coin cells. A Celgard®-3501 separator and 150 µL of 1 M LiPF₆ in ethylene carbonate (EC) ethyl methyl carbonate (EMC) (3:7) electrolyte (from Solvionic, Toulouse, France) are utilized. The components were assembled in a glove box filled with argon ($O_2 < 0.1$ ppm, $H_2O < 0.1$ ppm). The coin cells were electrochemically characterized with a BioLogic VMP3 potentiostat (Grenoble, France). All cells are assembled with the same batch of electrolyte, with the same procedure in the same glove box by the same person to avoid any undesired variations in the experiment.

Electrochemical impedance spectroscopy (EIS) measurements of the cells were performed with an AC amplitude of 10 mV and a frequency range of 200 kHz to 10 mHz. The Nyquist plot was recorded at open circuit voltage (OCV) after assembling and every hour until impedance stabilization was observed.

The galvanostatic stripping-plating cycle of the Li/Li symmetrical cells was recorded with different current densities corresponding to C-rates of C/2, 1 C, 2 C, 3 C, 4 C, 5 C, and 10 C. Before cycling, a rest period was performed to stabilize the evolution of impedance (~40 h), monitored by EIS measurements. The areal capacity was set to 0.5 mAh·cm⁻² and the limit voltages were set at ±3 V. The cycling protocol consists of one cycle at C/2, followed by three cycles for all the C-rates and finally ten cycles at 10 C. Long-term stability experiments were performed at 2 C (i.e., 1 mA·cm⁻²) just after impedance stabilization. The cycle was allowed to proceed until cell death.

At least three cells were assembled for each sample and electrochemical test. When a cell presents an evident failure or unusual cycling behavior in comparison to others, due to a problem during assembling for instance, the cycling result was not considered in the statistical distribution of the data.

3. Results and Discussion

3.1. Physical Characterizations of Li Foils

The surfaces of Li foils were first observed with an SEM microscope. Figure 2 shows SEM morphological images at a magnification of (a–c) $\times 100$ and (d–f) $\times 10,000$ for (a,d) Lithium HQ, (b,e) Lithium #1 and (c,f) Lithium #2 foils (t_0 samples). At low magnification, the surface of Lithium HQ (Figure 2a) appears uniform and relatively flat, and the boundaries of the Li grains are clearly visible. In contrast, for Lithium #1 (Figure 2b), a thick and inhomogeneous protective or artificial layer is present on Li surface, and it appears to be cracked in several places. There seems to be more mechanical stress for this sample in comparison with the others. The surface of Lithium #2 (Figure 2c) is characterized by pronounced lamination marks that increase the surface roughness. Nevertheless, grain boundaries are still visible but less marked than for Lithium HQ. In addition, a residual organic impurity (the black lines in the SEM image of Figure 2c) is observed on the surface; it could be a residue coming from the lamination process either to facilitate the lamination process or to protect the Li surface. Generally, more contaminants are observed at the surface of Lithium #1 and #2 sheets in comparison with the Lithium HQ sample. By increasing the magnification, different features are observed on the surface for the three Li foils. Firstly, small white spots are observed on the Lithium HQ surface; they are slightly more conductive and appear like holes dug in the metal. Most probably it could be fresh or less oxidized Li metal. Similar observation at high magnification is done for Lithium #1 except the surface is more accidented, with a lot of cracks, and resembles a thin ceramic layer. Elemental mappings of C, Li, and O for the three Li sheets are presented in Figure S2. There is no clear variation of composition between the surface of Lithium HQ (black part) and the white spots. However, it is more evident for Lithium #1 (see Figure S2e–h), where the mapping of oxygen shows the spots are less concentrated in O and C that presumes it be Li metal.

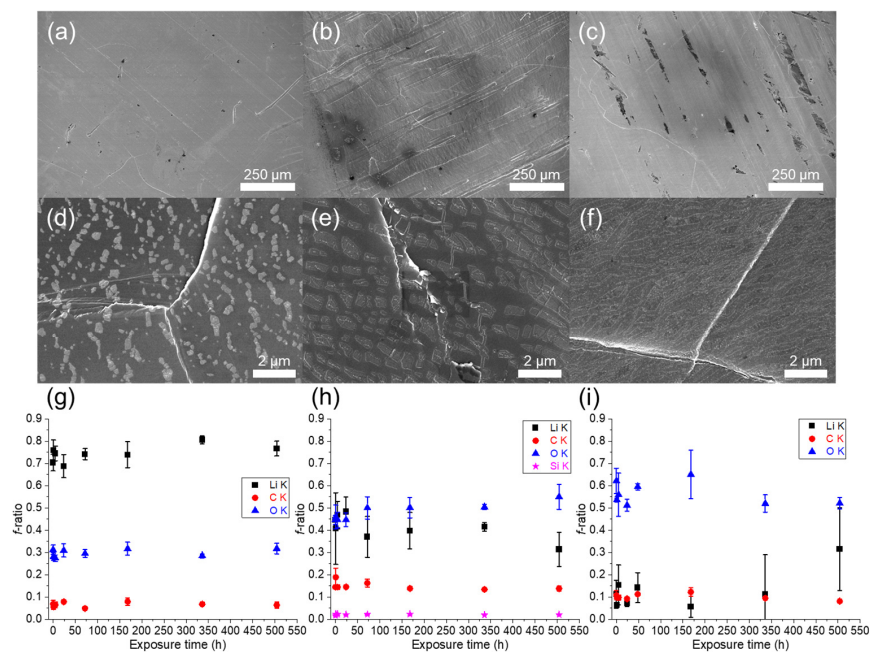


Figure 2. SEM images at a magnification of (a–c) $\times 100$ and d–f $\times 10,000$ for (a,d) Lithium HQ, (b,e) Lithium #1 and (c,f) Lithium #2 foils (t_0 samples). The scale is indicated by the white bars. Variation of chemical composition (C, O, Li, Si) as a function of exposure time in dry room for (g) Lithium HQ, (h) Lithium #1 and (i) Lithium #2. Data are obtained from EDX analysis.

It is quite hard to know with certitude the origin of these white spots on the Li surface, but it might be tentatively explained by the nature of lithium metal itself. Metals have a natural tendency to oxidize in the atmosphere, even in the absence of humidity. A thin oxide layer is formed on the metal surface, and for some metals such as aluminum, this layer protects the metal from further oxidation because its compactness impedes the contact between the atmosphere and the unprotected metal. However, for some metals such as lithium, the oxide layer cannot protect the metal. In corrosion, this feature is well known and can be anticipated by calculating the so-called Pilling-Bedworth ratio (PBR) value of the oxide film [16]. Essentially, a PBR ratio >2 does not protect the surface of the metal because the oxide layer chips off (such is the case for iron, for instance). When the PBR ratio is comprised between 1 and 2, then the oxide layer confers a stable protection on the metal (e.g., aluminum or chromium). Lastly, PBR values inferior to 1 yield porous and broken films that cannot effectively protect the metal surface [17]. In the case of Li metal, the native layer formed on the surface is mostly composed of Li_2O that can further react with H_2O and CO_2 to generate LiOH and Li_2CO_3 . The PBR value for Li_2O is about 0.57 and inevitably a porous oxide film will be formed that will expose fresh Li—as observed, for instance, with Mg-Li-Ca alloys by Zeng et al. [18].

The high magnification SEM image of the surface for Lithium #2 foil (Figure 2f) shows a different behavior. In fact, the entire surface of the metal is covered with small particles rich in oxygen. Figure S3 gives a comparison of morphological and composition images for Lithium HQ and Lithium #2 sheets that confirms the surface homogeneity for the in-house Li while strong variations in chemistry are observed for Lithium #2. Cracks are visible (fresh Li metal), and the quasi-spherical particles are mainly composed of oxygen.

Then, the chemical composition and its variation in function of exposure time in dry room for the three Li foils was monitored by EDS spectra. Figure S4 presents typical EDS spectra (five measures) acquired on the Li surface. Several measures were performed for each sample. The data were then compiled to follow the evolution of the different atoms' concentration during aging in air for the three Li foils; the results are shown in Figure 2. Firstly, the surface for all the Li foils is composed of C, O, and Li except Si impurity is detected for Lithium #2. The concentration in atoms is normalized by representing the *f*-ratio for each element. This is a relatively new quantitative X-ray microanalysis method that gives the composition of a sample [19]. In addition, samples can be easily compared between them. The surface of the in-house Li metal (Figure 2g) is mainly composed of Li with a small quantity of oxygen and carbon coming from the native passivation layer. The composition seems relatively uniform on the surface of the sample, as demonstrated by the small error bars. This is in good accordance with SEM images showing a clean surface. The surface of Lithium #1 is characterized by a high amount of oxygen and carbon, which suggests the presence of an artificial Li_2CO_3 layer [20]. This hypothesis seems supported by the brittleness and the high surface roughness of this layer, as evidenced below with hardness measurements (Figure 3) and by the optical and 3D laser scanning confocal images (Figure S5). Strangely, the surface for Lithium #2 is mainly composed of oxygen, which is present in a higher concentration than for Lithium #1. Again, this seems supported by SEM observations, which show small, oxidized particles all over the Li metal surface (see Figure 2f and Figure S3e in the Supporting Information). This surface composition as well as the organic residue observed on the surface at low magnification (Figure 2c) reveal the presence of an artificial layer intentionally added either to protect the metal from uncontrolled oxidation or simply coming from the lamination process.

Generally, the exposure in dry room for three weeks does not drastically change the surface composition for the three Li metal foils—even if some slight variations are observed from one sample to another, especially for Lithium #2. In terms of data distribution that is an indication of the surface homogeneity, the commercial Li foils presented the higher disparity in value in comparison to Lithium HQ. The values for O and Li contents varied significantly for a measure to another for a same sample, confirming the chemical composition of the surface is not uniform. The more stable sample, in terms of composition upon exposure

time in dry room, remains the Lithium HQ. The effect of aging is not really appreciated, and the same conclusion is stated following the results from hardness measurements and electrochemical tests discussed below.

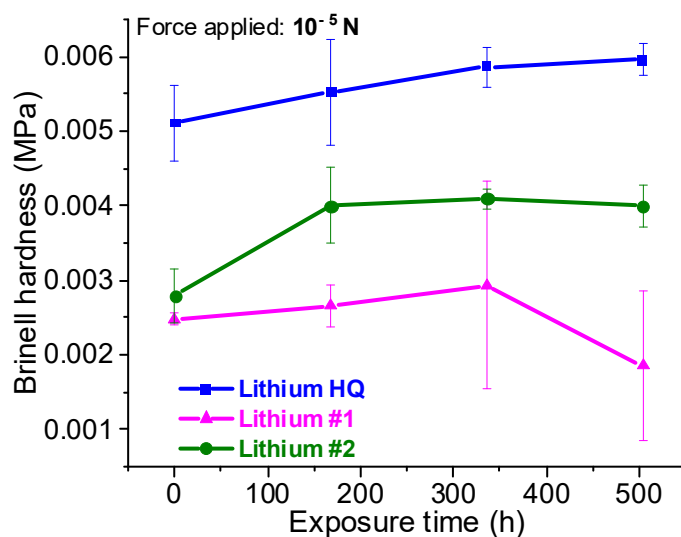


Figure 3. Evolution of Brinell hardness as a function of exposure time in the dry room for the three samples of Li metal foils.

A simple method has been developed for bringing out the difference in hardness property at the surface of Li, which can reveal the presence of protecting or artificial passivation layers generated during the Li rolling process. Indentation marks are produced on the Li surface using a DMA machine equipped with a spherical indenter tip (see Figure 1). The Brinell hardness number is determined by solving Equation (2) and is correlated to the diameter of the indentation mark. In summary, the smaller the diameter, the less the tip penetrates inside the Li, which means a harder surface. Figure 3 shows the evolution of Brinell hardness as a function of exposure time in dry room for the three Li metal foils. The Lithium HQ sample has a higher value of hardness, comprised between 5×10^{-3} and 6×10^{-3} MPa. For Lithium #2, the values are comprised between 3×10^{-3} and 4×10^{-3} MPa, indicating a softer surface than pure Li metal and in accordance with the presence of a thick and soft protection or polymer layer, which is easily deformable. Lithium #1 is characterized by the lowest value of Brinell hardness (2.5×10^{-3} MPa), which could be explained by the presence of a brittle inorganic layer as evidenced by SEM and confocal microscopy observations. Optical and 3D laser scanning confocal images for the three Li foils are presented in Figure S5. The indentation marks are clearly visible for the Lithium HQ but hardly discernable for the two commercial Li foils. In addition, the surface roughness for Lithium #1 and #2 has a large variation and reaches up to $\pm 5.5 \mu\text{m}$, whereas for Lithium HQ a relatively flat surface is observed. The reproducibility of Brinell hardness measurements for Lithium #1 seems to be less good than for other Li foils due to the poor surface quality and the presence of an inhomogeneous artificial layer.

Although this method is interesting for comparing Li samples, no clear evolution of the Brinell hardness upon exposure time in dry room was observed for all the Li foils. If a severe oxidation of the surface would appear, then a gradual decrease of the Brinell hardness would be observed. Thus, three weeks of exposition do not seem to severely oxidize the surface of the Li foils, at least in this well-controlled dry room. It should be noted that the native passivation is already present for the three lithium samples depending on the method of manufacture, which can be a good protection barrier.

EBSD is a microstructural characterization technique that provides crystallographic information for a sample directly in an SEM. The diffraction pattern generated is analyzed to determine different characteristics such as grain size, texture, and crystal orientation [21]. The analysis was performed only for the Lithium HQ and Lithium #2. Due to the thick

passivation layer on the Lithium #1 surface, the EBSD analysis was not performed. The results are available under Supporting Information (see Figures S6 and S7) and showed that larger grains are obtained for Lithium #2 in comparison with Lithium HQ. We cannot conclude at this stage if grain size has an influence on electrochemical properties because another complete study should be performed by comparing several Li metal sheets with various grain size distributions and orientations. It is important to keep in mind that battery performance could be affected by numerous parameters such as the nature and thickness of the passivation layer, the size of the grains, and the orientation of the crystals, as well as by any impurities in the composition of the Li anode [22].

3.2. Electrochemical Results and Cell Performance Comparison of Li Foils

3.2.1. Electrochemical Impedance Spectroscopy

To correctly benchmark the different lithium foils, they were also electrochemically tested with three protocols. Firstly, symmetric Li/Li cells were assembled and kept at OCV while the evolution of the total resistance was monitored by EIS. Figure 4a shows the typical Nyquist plot for a symmetric Li/Li cell assembled with the Lithium HQ exposed to the dry room atmosphere for one week. Every hour, an impedance spectrum is recorded until stabilization. The diameter of the capacitive semicircle is mostly related to the interfacial resistance of the electrolyte with the Li electrodes [23]. The impedance gradually increases during storage at OCV until it stabilizes after about 40 h. This behavior is well known and attributed to the growth of a passivation layer on the Li surface due to side reactions between organic solvents and Li metal resulting in the formation of the so-called solid electrolyte interface (SEI) [24]. When a stable SEI is formed on the Li anodes, the impedance becomes stable. This test was performed, on the one hand, to know the optimal time to be applied before the stripping/plating experiments and to compare the total resistance for the different Li foils. After cell assembly, the Lithium HQ sample exposed to the dry room atmosphere for one week (see Figure 4a), shows a total resistance of approximately $270\ \Omega$ and reaches $\sim 740\ \Omega$ after 40 h. This result is consistent with data reported by Wellmann et al., for instance, for symmetric Li/Li cells assembled with the same liquid electrolyte, showing similar resistances both after assembling and stabilization [25]. All the impedance spectra for the three Li foils investigated in this study, after stabilization for different exposure times in the dry room, are plotted in Figures S8–S10 in the Supporting Information. From this data, the total resistance is plotted against exposure time in a dry room for the three Li sheets shown in Figure 4b.

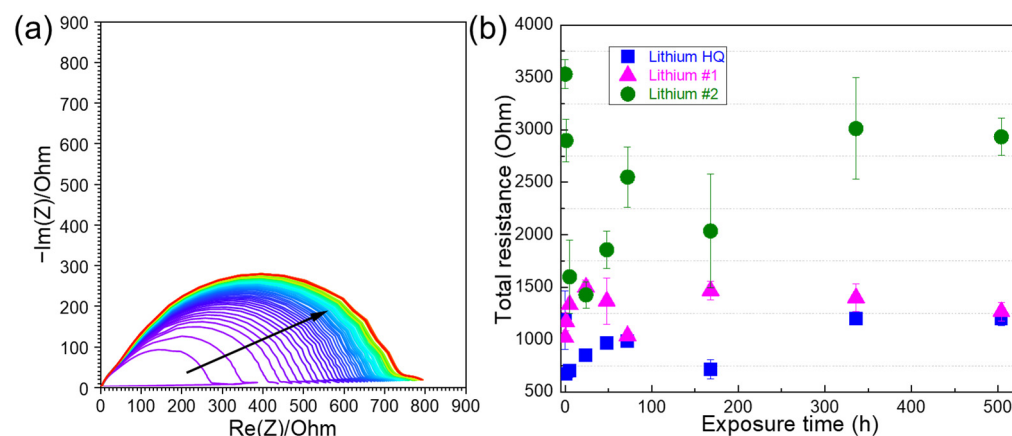


Figure 4. (a) Nyquist plots for a symmetric Li/Li cell assembled with Lithium HQ exposed to the dry room atmosphere for one week. Impedance spectra are recorded every hour. The black arrow shows the increase of impedance over time until stabilization. (b) Evolution of the total resistance determined from Nyquist plots after impedance stabilization for the three Li metal foils.

Based on the physical characterization above, it is obvious that cells assembled with Lithium HQ electrodes present the lowest total resistance. Even if some variations of

resistance value are obtained after stabilization for the cells made with the same Li, the error bars for Lithium HQ samples are quite small in comparison to those obtained for Lithium #1 and Lithium #2. This is consistent with the results from confocal laser scanning and SEM analyses and surface compositions discussed above, demonstrating the superior quality and performance of Lithium HQ. The nature of passivation layer of Lithium #1 is clearly different from that of Lithium HQ, which is probably composed of Li_2CO_3 [20]. Thus, the total resistance for the cells made with Lithium #1 will necessarily be higher and the reproducibility is worse (see error bars). This is due to the poor structural and chemical inhomogeneity at the surface of this Li, which leads to variations in electrochemical performance from one cell to another. Lastly, the cells assembled with the Lithium #2 electrodes showed the highest total resistance values, either for the t_0 sample or those exposed for three weeks in the dry room. In addition, their reproducibility is worse than the cells made with Lithium #1. Since the nature of the passivation layer is not known for Lithium #1 and #2, it is difficult to pinpoint the reason why Lithium #2 gave the highest resistance. We assume it comes from a thick, soft layer on this lithium, resulting in more side reactions with electrolyte to form a resistive SEI layer. This soft layer unavoidably leads to more resistance during the stripping/plating process, which will be confirmed below with galvanostatic cycling experiments.

This first electrochemical test allows us to easily compare the Li foils with each other, but the trend of the evolution of the total resistance upon exposure time in dry room is not conclusive. This accords with the characterization results, which did not show any increase of carbon or oxygen content at the surface of the initially anticipated exposed Li foils. In fact, long-term exposure in the air would favor the generation of Li_2CO_3 , LiOH , and Li_2O and therefore would increase the impedance. Even in a glove box under argon with a low degree of contamination, this phenomenon was also observed by Otto et al., but over several weeks of exposure [6]. One possible reason could be the good dry room conditions with a low dew point (see Figure 1a) and the relatively short duration of the experiment (three weeks), which did not allow time to appreciate a clear change of chemical composition and then induce an increase of impedance. Secondly, as well discussed in the study by Otto et al., perhaps the Li-containing species formed upon exposure are soluble in liquid electrolyte and their effect is missed, but that does not explain why they are not detected by EDX analysis. The effect of Li aging with a solid electrolyte is more severe than with liquid electrolytes because the components of the passivation layer can hardly dissolve in the electrolyte [6]. Thirdly, the native oxide layers instantly formed, or the protective layer applied on the Li surface during the rolling process efficiently protects the Li from subsequent oxidation, at least in a well-controlled environment such as the dry room used in this study and for short periods. Most probably, the reason for these observations is a combination of these assumptions.

3.2.2. Rate Capability

The second electrochemical test performed to compare the Li foils was a galvanostatic stripping/plating experiment by setting the areal capacity to 0.5 mAh.cm^{-2} . As an example, Figure 5a presents the voltage profile at different C-rates for three cells assembled with the Lithium HQ exposed to the dry room atmosphere for one week. Firstly, during the first charge, we observe a relatively high overpotential around 0.3 V. For all cells made with the Lithium HQ, the initial overpotential is quite similar, around 0.3–0.4 V. For further detail, all the data for this electrochemical test and for cells assembled with Lithium HQ exposed in dry room for different times are available in Figure S11. This behavior is due to the initial passivation layer where electrodeposition occurs, and afterward the overpotential decreases since the surface has been changed by the initial deposition of fresh Li metal [25]. The quality of Li surface strongly impacts the first deposition where the Li metal electroplates as mossy dendrites on the electrode surface due to inhomogeneous nucleation and growth. Surface defects have an evident impact on the first recorded overpotential and the more inhomogeneous the surface, the higher the overpotential. This is exactly what is observed for

Lithium #1 and Lithium #2, which present poor surface quality. Figures S12 and S13 present the corresponding electrochemical results for these two Li foils exposed for different times in dry room. Overpotentials of approximately 0.4–0.45 and 0.45–0.6 V were recorded during the first charge for Lithium #1 and Lithium #2, respectively. This observation is in accordance with the SEM results. When the stripping/plating current is increased to 1C (see Figure 5a), the shape of the galvanostatic cycling voltage profiles is in conformity with the model explained by Dasgupta and coworkers [26], for instance, for symmetric Li/Li cells in liquid electrolyte. The peak behavior is well observed, and the voltage instantly relaxes towards the OCV once the applied current is removed. At this stage, mossy lithium is generated as well as dead Li (coming from the strip of fresh mossy dendrites) forming a relatively thin decomposition layer on top of the lithium foil, one that does not impede Li-ion transport. Upon cycling, this inhomogeneous Li stripping/plating gradually develops high surface area lithium (HSAL) and therefore the applied areal current density is reduced, which inherently decreases the overvoltage. This behavior is observed for all the cycling rates investigated in this study and clearly highlighted in Figure 5b by representing the average voltage during cycling. At each C-rate, three cycles were performed, and an obvious reduction in the average voltage is observed, confirming the continuous formation of HSAL. Similar results are often reported in the literature on the cycling of symmetric Li/Li cells at various C-rates [27,28]. For long-term cycling, the shape of the galvanostatic curve and the overvoltage value evolve differently and will be discussed below with long-term cycling experiments at 2 C. The results presented in Figure 5 demonstrate the good reproducibility of the stripping/plating cycles of Li for the three cells made with Lithium HQ exposed in dry room for one week. In addition, the cycling is well defined without fluctuations or sharp voltage drop confirming the absence of dendrites. The same observation is valid for all the cells made with Lithium HQ exposed to different times (see galvanostatic curves in Figure S11). For the two other tested Li foils, the electrochemical results are strongly impacted by the poor quality of the passivation layer. Figure 5c presents the evolution of the average overpotential during the charges for all the C-rates and for the three Li metal foils exposed in dry room for different exposure times. This simple representation again clearly shows the superior quality of Lithium HQ in comparison with Lithium #1 and Lithium #2 samples. The higher the overpotential, the more difficult it is to achieve the plating/stripping process, which is in good agreement with impedance results (Figure 4b). Looking more closely at the rate capability graphs obtained for Lithium #1 up to 1 C (Figure S12 in Supporting Information), the cycling is relatively similar to that of Lithium HQ cells but with higher polarization. In contrast, at higher currents of 2C and above, the voltage hysteresis of Li plating/stripping gave rise to random voltage oscillations, which are mainly derived from the instability of the Li/electrolyte interface [28]. However, no abrupt voltage drop from high to lower potentials is observed in the voltage profile, such as would normally be attributed to dendrites-induced short circuits [27,29]. Statistically, with all symmetrical cells made with Lithium #2 foil, the average charging overpotential is higher than for cells assembled with Lithium HQ and Lithium #1 as shown in Figure 5c. Nevertheless, the voltage profiles are well defined up to 5 C without any voltage oscillations, which on the other hand start to appear at 10 C for almost all cells. Thus, the behavior of the coin cells made with the two foils of commercial lithium metal is strongly affected by the nature of the passivation layer. In fact, it is not the Li metal with the highest impedance (i.e., Lithium #2) that first fails to cycle at high C-rates (i.e., Lithium #1). In summary, symmetrical cells assembled with Lithium HQ, Lithium #1 and Lithium #2 cycled correctly without voltage oscillations or signs of dendrites up to 10 C, 1 C, and 5 C, respectively.

3.2.3. Long-Term Cycling

The third electrochemical test is defined by a long-term cycling protocol at a rate of 2 C until the battery is dead. Figure 6a presents the typical cycling for two assembled Lithium HQ cells exposed to the dry room atmosphere for one week. The cycling corresponds perfectly to the work reported by Dasgupta and coworkers [26], which describes each stage of the Li/Li batteries cycle. As explained above, during the first cycles, the overpotential

decreases slightly due to the formation of HSAL, which decreases the actual areal current density. The overpotential profile starts to increase with cycling and evolves from a peak behavior to the formation of an arc shape, which is associated with the formation of a thick dead Li layer. Lastly, at the end of cycling, anarchic voltage fluctuations are recorded that suggest electrolyte consumption or formation of micro-short circuits in the cell [25,28]. When the average potential begins to increase rapidly, as shown in Figure 6b, then the cells are stopped, and this behavior is considered a failure mode. Subsequently, the voltage dropped sharply, which can be attributed to a hard short circuit [27,29]. All the long-term cycling results for the cells made with different Li foils are available in Figures S14–S16. The number of cycles performed at 2 C before failure is shown in Figure 6c as a function of exposure time in a dry room. The impedance results, analyzed previously, are not conclusive to the evolution of the total resistance as a function of the exposure time in a dry room. The same conclusion is reached with the number of cycles at 2 C before failure. On the other hand, from a statistical point of view, it can easily be concluded that cells made with Lithium HQ present a better durability than those made with Lithium #1 and Lithium #2. Moreover, the cycling with the two commercial Li foils is more polarized and noisier (see Figures S15 and S16) than with cells assembled with the in-house Li metal (Figure S14).

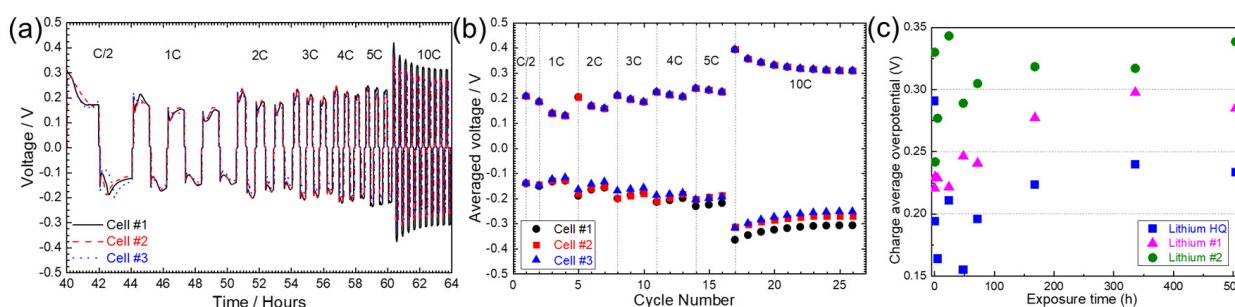


Figure 5. (a) Rate capability at different C-rates and (b) averaged voltage obtained for three cells assembled with the Lithium HQ exposed to the dry room atmosphere for one week. (c) Evolution of the average overpotential during the charges for all the C-rates and for the three Li metal foils exposed in dry room for different exposure times.

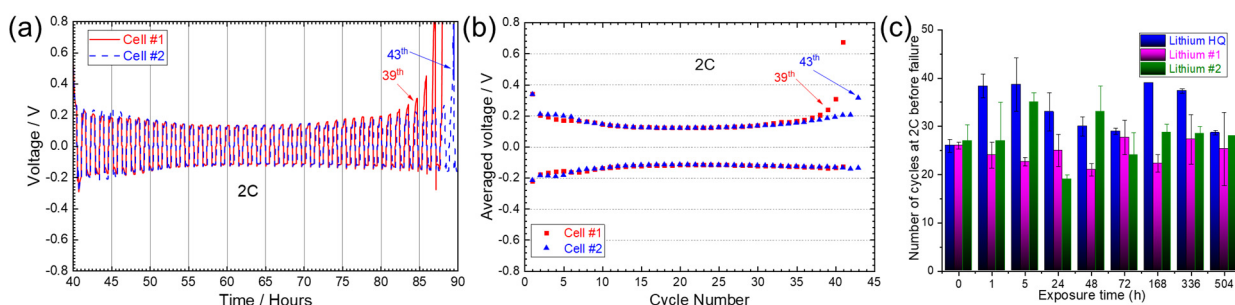


Figure 6. (a) Long-term stability at 2 C and (b) averaged voltage obtained for two cells assembled with the Lithium HQ exposed to the dry room atmosphere for one week. Cells died at the 39th and 43rd cycles. (c) Number of cycles at 2 C before failure as a function of exposure time in dry room for the three Li metal foils.

Table 1 summarizes the electrochemical and characterization results obtained for the three Li metal foils. The in-house Li metal clearly exhibits the best surface quality, either in surface composition homogeneity or in surface topography such as absence of contaminations and well-defined Li grain boundaries. The worst sample is Lithium #1, which presents a thick and inhomogeneous layer rich in oxygen and carbon, such that it was impossible to perform EBSD analysis for this sample. The Brinell hardness measurement confirms this result by revealing a brittle inorganic layer on the surface of this lithium metal. Finally, the electrochemical performances are in good agreement with the characterization results. Lithium #2 presents

intermediate electrochemical performance and surface quality. Even though this lithium shows a higher total resistance after stabilization, it still supports higher stripping/plating currents than Lithium #1. It is worth noting that in terms of the reproducibility of experimental data—and it is true either for morphological or electrochemical results—Lithium HQ is the best sample among the three investigated in this study.

Table 1. Summary of the electrochemical and characterization results for the three Li foils studied. The Rate capability column reports the critical current density; the 2 C stability column reports the highest cycle number obtained with the average number of cycles in parentheses; the Total resistance (Ω) column reports the range of resistance. The average Brinell hardness and surface roughness are reported. Comments on surface aspect and composition are also added.

	Electrochemical Results				Characterizations		
	Rate Capability	2 C Stability	Total Resistance (Ω)	Brinell Hardness (MPa)	Surface Roughness	Surface Aspect	Surface Composition
Lithium HQ	10 C	45 (34)	680–1200	5×5.10^{-3}	$\pm 1.5 \mu\text{m}$	Smooth surface, well-defined Li grain boundaries	Homogeneous, mainly composed of Li, small quantity of oxygen
Lithium #1	1 C	32 (25)	1020–1500	2.5×10^{-3}	$\pm 5.5 \mu\text{m}$	Accidented and brittle surface, no Li grains visible	Inhomogeneous, high concentration of oxygen and carbon, silicon as an impurity, unknown contaminants
Lithium #2	5 C	38 (28)	1430–3530	3.7×10^{-3}	$\pm 4.5 \mu\text{m}$	Large furrows and lamination marks, fractures, Li grains hardly visible	Inhomogeneous, high concentration of oxygen, unknown contaminants

4. Perspectives

Although the results obtained during the Li aging experiment in the dry room were not very concluding, these tests are critical because the manufacture of batteries using the Li anode will inevitably be conducted in such an environment, so the effect of a prolonged exposure to low relative humidity must be known. This experimental plan can be easily reproduced by other researchers to characterize their own in-house alloys or Li anodes.

However, one of the most difficult parameters to control for the current benchmarking method of Li (see Scheme 1) is the determination of the time “ t_0 ”. Ideally, the sample t_0 to be considered should be the Li foil directly extracted after rolling, where the surface exposure time is almost zero. In practice, that is clearly impossible, and it is even more true for commercial Li because the fabrication, conditioning, and shipping processes are uncontrolled. However, this approach is not completely accurate, given the instantaneous passivation layer present on the Li surface. To properly appreciate the effect of exposure time in a dry room, this validation method must be performed on cleaner Li. Moreover, the dry room where the experiment is conducted should have a well-controlled atmosphere with a dew point continuously below -50°C . Usually, when the lithium surface starts to severely oxidize, it turns black or even grey, but no such color change was observed during the experiment. In fact, at the beginning of the experiment, a sample of each Li was exposed to the dry room atmosphere, and they were recorded on video together for 3 weeks (~498 h). The video is available in the Electronic Supplementary Information. No obvious change in color or appearance was observed for the three Li metal foils (PT: Lithium HQ, PA.c: Lithium #1 and PA: Lithium #2), which confirms that the usual dry room conditions are appropriate for lithium manipulation.

It is worth noting that the results and conclusions could have been different if a different electrolyte had been used, particularly a solid-state electrolyte since the wetting between Li metal and the solid electrolyte can strongly affect the performance [30–32]. Moreover, with the solid electrolyte, it is difficult to dissolve the native SEI layer. The results of this experimentation could also be strongly affected by the quality of the dry room since Li metal is very sensitive to humidity. In the case of commercial Li foils, due to

the uncontrolled manufacturing, packaging, and shipping processes, a native passivation layer is already formed when they are received, complicating interpretations or conclusions during aging experiments.

Finally, a lot of parameters can affect the electrochemical performance and must also be considered when designing a comparative study. To compare several sources of Li metal, the thickness of the Li metal foils must be identical since this parameter can impact the cyclability of the cells [13]. In this paper, self-supported Li foils with the same thickness (~45 μm) were used. The process of fabrication is probably one of the most important factors as it could generate various structures and sizes of Li grains. For instance, the size of Li grains can be easily tuned via extrusion and rapid molding processes [10] and it is well known that the size of Li grains impacts the mechanical [10,12] and electrochemical performances. Recently, Mehdi et al. demonstrated that large grains are more desirable for high Coulombic efficiency values, while small randomly interconnected grains are not [22]. In contrast, a porous layer morphology was achieved for Li metal anode fabricated by plasma vapor deposition [11], while a nanorods similar to morphology can be obtained for electrodeposited Li anodes [7]. Other parameters such as impurities inside the Li foil (e.g., Si) as well as the thickness of the passivation layer and the nature of the protective layer (natural or artificially added during the lamination process) are strong factors to consider when comparing samples.

From a general point of view, researchers must be very careful with experimental conditions when comparing performance of their materials or electrochemical systems with others. In this regard, this study provides practical experimental tools to compare different lithium metal anodes quantitatively and to validate their quality during storage or from different production batches.

5. Conclusions

In this paper, we proposed a simple benchmarking method with the aim of evaluating and comparing the quality and electrochemical performance of different sources of Li anodes. Our in-house Li metal foil (Lithium HQ) was compared to two commercial foils (Lithium #1 and Lithium #2). SEM observations coupled with EDX analysis showed the Lithium HQ sample had the best surface quality while both Lithium #1 and #2 presented a thick and inhomogeneous passivation layer. It seems Lithium #1 possesses an inorganic layer such as Li_2CO_3 that could be generated during the lamination process under CO_2 -rich atmosphere [33]. In contrast, the surface of Lithium #2 seems to have a protective treatment and the surface is highly concentrated in oxygen.

Based on approximately 285 coin cells that were assembled in this study with the three lithium foils, the conclusion, without doubt, is that Lithium HQ gave the best electrochemical performance. Cell performance seems to be strongly related to the quality and uniformity of the Li surface, which is a dependent consequence of its fabrication method.

The benchmarking method proposed in this research paper included the effect of Li aging in a dry room on the electrochemical performance. We also proposed to follow the chemical composition by EDS of the Li foils surface after exposition in dry room. Surprisingly, the chemical composition as well as the electrochemical performance for all the Li anodes remain quasi unchanged upon time of exposition in dry room. This behavior could be due to the good dry room conditions with a low dew point and the relatively short duration of the experiment (i.e., three weeks), which did not allow time to appreciate a clear change of chemical composition. Another possible reason would be that the native oxide layers instantly formed, or the protective layer applied on the Li surface during the rolling process efficiently protects the Li from subsequent oxidation.

In conclusion, we proposed a facile benchmarking method to compare Li anodes, which can be easily reproduced by other research groups, especially the electrochemical evaluation that uses a widely spread coin-cell format. Such a method should be widely used by researchers in the field of energy storage and especially for those working in the development of Li metal and all-solid-state batteries. Since the metal anode is believed to

be the future negative electrode of ASSB, a kind of “standard” method for its evaluation must be adopted as soon as possible.

Supplementary Materials: The following supporting information can be downloaded at: <https://www.mdpi.com/article/10.3390/batteries9070368/s1>, Figure S1: Correlation between the relative humidity (%) and the dew point (°C) in a room temperature of 21 °C. The equation can be used to easily convert the dew point temperature into percentage of relative humidity; Figure S2: (a,e,i) SEM images and corresponding elemental mappings of (b,f,j) Li, (c,g,k) C and (d,h,l) O for (a–d) Lithium HQ, (e–h) Lithium #1 and (i–l) Lithium #2 (t0 samples). The scale is indicated by the white bars; Figure S3: (a,c,e) SEM morphological and (b,d,f) composition images for (a,b) Lithium HQ and (c–f) Lithium #2 foils (t0 samples). The scale is indicated by the white bars; Figure S4: EDS spectra for the Lithium HQ foil exposed during 72 h in dry room. Five measures are made randomly on the Li metal surface; Figure S5: (a,c,e) Optical and (b,d,f) 3D laser scanning confocal images of (a,b) Lithium HQ, (c,d) Lithium #1 and (e,f) Lithium #2 surfaces. Indentation marks are visible in the middle; Figure S6: Crystallographic orientation of grains in inverse pole figures (IPF) in the z-axis obtained from EBSD analysis for (a) Lithium HQ and (b) Lithium #2. Acquisition was impossible for lithium #1 due to the poor surface quality; Figure S7: (a) Cumulative number of Li grains as a function of Li grain diameter for Lithium HQ and Lithium #2. (b) Cumulative percentage of Li grains as a function of Li grain diameter for Lithium HQ and Lithium #2. The average (Avg), minimum (Min) and maximum (Max) diameters of Li grains for each Li foil are given. Data is collected from EBSD inverse pole figure (IPF) maps; Figure S8: Electrochemical impedance spectra, after stabilization, recorded for cells made with Lithium HQ foils exposed in dry room atmosphere for different time periods; Figure S9: Electrochemical impedance spectra, after stabilization, recorded for cells made with Lithium #1 foils exposed in dry room atmosphere for different time periods; Figure S10: Electrochemical impedance spectra, after stabilization, recorded for cells made with Lithium #2 foils exposed in dry room atmosphere for different time periods; Figure S11: Results of galvanostatic stripping/plating cycling experiment for cells made with Lithium HQ foils exposed in dry room atmosphere for different time periods; Figure S12: Results of galvanostatic stripping/plating cycling experiment for cells made with Lithium #1 foils exposed in dry room atmosphere for different time periods; Figure S13: Results of galvanostatic stripping/plating cycling experiment for cells made with Lithium #2 foils exposed in dry room atmosphere for different time periods; Figure S14: Results of long-cycling experiment at 2C for cells made with Lithium HQ foils exposed in dry room atmosphere for different time periods; Figure S15: Results of long-cycling experiment at 2C for cells made with Lithium #1 foils exposed in dry room atmosphere for different time periods; Figure S16: Results of long-cycling experiment at 2C for cells made with Lithium #2 foils exposed in dry room atmosphere for different time periods.

Author Contributions: N.D.: conceptualization; formal analysis; investigation; methodology; supervision; project administration; validation; visualization; writing—original draft; writing—review and editing. A.P.: data curation; formal analysis; investigation; validation; visualization. M.L.: resources; investigation. J.M.: resources; investigation. S.C.-M.: resources; methodology; investigation. D.R.: resources; investigation. H.D.: resources; investigation. D.C.: resources; investigation. A.G.: conceptualization; visualization; writing—original draft. C.K.: conceptualization; visualization. All authors have read and agreed to the published version of the manuscript.

Funding: This work was financially supported by Hydro-Québec.

Data Availability Statement: Not applicable.

Acknowledgments: The laboratory experiments were conducted at the Center of Excellence in Transportation, Electrification, and Energy Storage (CETEES). The authors thank Hugues Levesque and Sylvain Martel for providing the Lithium HQ.

Conflicts of Interest: The authors declare no conflict of interest.

References

1. Stéphanie, B.; Fernandez, P.A.; Christophe, M.; Uwe, R.; Brent, W.; Laszlo, V.; Davide, D.A.; Thomas, S. *Net Zero by 2050. A Roadmap for the Global Energy Sector*; International Energy Agency: Paris, France, 2021; Available online: <http://iea.li/nzeroadmap> (accessed on 6 May 2023).
2. Doughty, D.H.; Roth, E.P. A General Discussion of Li Ion Battery Safety. *Electrochem. Soc. Interface* **2012**, *21*, 37–44. [CrossRef]
3. Sun, Y.-K. Promising All-Solid-State Batteries for Future Electric Vehicles. *ACS Energy Lett.* **2020**, *5*, 3221–3223. [CrossRef]

4. Rosso, M.; Brissot, C.; Teyssot, A.; Dollé, M.; Sannier, L.; Tarascon, J.-M.; Bouchet, R.; Lascaud, S. Dendrite Short-Circuit and Fuse Effect on Li/Polymer/Li Cells. *Electrochim. Acta* **2006**, *51*, 5334–5340. [[CrossRef](#)]
5. Zhang, Y.; Zuo, T.-T.; Popovic, J.; Lim, K.; Yin, Y.-X.; Maier, J.; Guo, Y.-G. Towards Better Li Metal Anodes: Challenges and Strategies. *Mater. Today* **2020**, *33*, 56–74. [[CrossRef](#)]
6. Otto, S.K.; Fuchs, T.; Moryson, Y.; Lerch, C.; Mogwitz, B.; Sann, J.; Janek, J.; Henss, A. Storage of Lithium Metal: The Role of the Native Passivation Layer for the Anode Interface Resistance in Solid State Batteries. *ACS Appl. Energy Mater.* **2021**, *4*, 12798–12807. [[CrossRef](#)]
7. Porthault, H.; Decaux, C. Electrodeposition of Lithium Metal Thin Films and Its Application in All-Solid-State Microbatteries. *Electrochim. Acta* **2016**, *194*, 330–337. [[CrossRef](#)]
8. Vanleeuw, D.; Sapundjiev, D.; Sibbens, G.; Oberstedt, S.; Salvador Castañera, P. Physical Vapour Deposition of Metallic Lithium. *J. Radioanal. Nucl. Chem.* **2014**, *299*, 113–1120. [[CrossRef](#)]
9. Hovsepian, B. Rolling of Lithium. U.S. Patent 3721113A, 20 March 1973.
10. Somekawa, H.; Nishikawa, K.; Moronaga, T.; Ohmura, T. Fabrication of Li Anode Metal via Bulk Mechanical Property Analysis. *J. Power Source* **2023**, *569*, 233019. [[CrossRef](#)]
11. Saager, S.; Decker, L.; Kopte, T.; Scheffel, B.; Zimmermann, B. High-Performance Anodes Made of Metallic Lithium Layers and Lithiated Silicon Layers Prepared by Vacuum Technologies. *Batteries* **2023**, *9*, 75. [[CrossRef](#)]
12. Aspinall, J.; Armstrong, D.E.J.; Pasta, M. EBSD-Coupled Indentation: Nanoscale Mechanics of Lithium Metal. *Mater. Today Energy* **2022**, *30*, 101183. [[CrossRef](#)]
13. Niu, C.; Liu, D.; Lochala, J.A.; Anderson, C.S.; Cao, X.; Gross, M.E.; Xu, W.; Zhang, J.-G.; Whittingham, M.S.; Xiao, J.; et al. Balancing Interfacial Reactions to Achieve Long Cycle Life in High-Energy Lithium Metal Batteries. *Nat. Energy* **2021**, *6*, 723–732. [[CrossRef](#)]
14. Hovington, P.; Timosheskii, V.; Burgess, S.; Demers, H.; Statham, P.; Gauvin, R.; Zaghib, K. Can We Detect Li K X-ray in Lithium Compounds Using Energy Dispersive Spectroscopy? *Scanning* **2016**, *38*, 571–578. [[CrossRef](#)]
15. Brodusch, N.; Demers, H.; Gauvin, R. Developments in Field Emission Gun Technologies and Advanced Detection Systems. In *Field Emission Scanning Electron Microscopy*; SpringerBriefs in Applied Sciences and Technology; Springer: Berlin, Germany, 2018.
16. Jiang, Q.; Lu, D.; Liu, C.; Liu, N.; Hou, B. The Pilling-Bedworth Ratio of Oxides Formed From the Precipitated Phases in Magnesium Alloys. *Front. Mater.* **2021**, *8*, 761052. [[CrossRef](#)]
17. Song, B.M.; Park, H.E.; Yoon, W.Y. Surface Control of Lithium Powder by Use of a DET. *J. Korean Phys. Soc.* **2009**, *54*, 1136–1140. [[CrossRef](#)]
18. Zeng, R.-C.; Sun, L.; Zheng, Y.-F.; Cui, H.-Z.; Han, E.-H. Corrosion and Characterisation of Dual Phase Mg–Li–Ca Alloy in Hank’s Solution: The Influence of Microstructural Features. *Corros. Sci.* **2014**, *79*, 69–82. [[CrossRef](#)]
19. Teng, C.; Gauvin, R. The F-Ratio Model for Quantitative X-Ray Microanalysis. *Talanta* **2021**, *235*, 122765. [[CrossRef](#)]
20. Zhuang, G.; Chen, Y.; Ross, P.N., Jr. The Reaction of Lithium with Carbon Dioxide Studied by Photoelectron Spectroscopy. *Surf. Sci.* **1998**, *418*, 139–149. [[CrossRef](#)]
21. Carneiro, I.; Simões, S. Recent Advances in EBSD Characterization of Metals. *Metals* **2020**, *10*, 1097. [[CrossRef](#)]
22. Mehdi, B.L.; Stevens, A.; Qian, J.; Park, C.; Xu, W.; Henderson, W.A.; Zhang, J.-G.; Mueller, K.T.; Browning, N.D. The Impact of Li Grain Size on Coulombic Efficiency in Li Batteries. *Sci. Rep.* **2016**, *6*, 34267. [[CrossRef](#)]
23. Shubha, N.; Prasanth, R.; Hoon, H.H.; Srinivasan, M. Plastic Crystalline-Semi Crystalline Polymer Composite Electrolyte Based on Non-Woven Poly(Vinylidenefluoride-Co-Hexafluoropropylene) Porous Membranes for Lithium Ion Batteries. *Electrochim. Acta* **2014**, *125*, 362–370. [[CrossRef](#)]
24. Nie, M.; Demeaux, J.; Young, B.T.; Heskett, D.R.; Chen, Y.; Bose, A.; Woicik, J.C.; Lucht, B.L. Effect of Vinylene Carbonate and Fluoroethylene Carbonate on SEI Formation on Graphitic Anodes in Li-Ion Batteries. *J. Electrochem. Soc.* **2015**, *162*, A7008–A7014. [[CrossRef](#)]
25. Wellmann, J.; Brinkmann, J.-P.; Wankmüller, B.; Neuhaus, K.; Rodehorst, U.; Hansen, M.R.; Winter, M.; Paillard, E. Effective Solid Electrolyte Interphase Formation on Lithium Metal Anodes by Mechanochemical Modification. *ACS Appl. Mater. Interfaces* **2021**, *13*, 34227–34237. [[CrossRef](#)] [[PubMed](#)]
26. Chen, K.-H.; Wood, K.N.; Kazyak, E.; LePage, W.S.; Davis, A.L.; Sanchez, A.J.; Dasgupta, N.P. Dead Lithium: Mass Transport Effects on Voltage, Capacity, and Failure of Lithium Metal Anodes. *J. Mater. Chem. A* **2017**, *5*, 11671–11681. [[CrossRef](#)]
27. Yang, M.; Jue, N.; Chen, Y.; Wang, Y. Improving Cyclability of Lithium Metal Anode via Constructing Atomic Interlamellar Ion Channel for Lithium Sulfur Battery. *Nanoscale Res. Lett.* **2021**, *16*, 52. [[CrossRef](#)]
28. Dai, H.; Gu, X.; Dong, J.; Wang, C.; Lai, C.; Sun, S. Stabilizing Lithium Metal Anode by Octaphenyl Polyoxyethylene-Lithium Complexation. *Nat. Commun.* **2020**, *11*, 643. [[CrossRef](#)] [[PubMed](#)]
29. Zou, P.; Wang, Y.; Chiang, S.-W.; Wang, X.; Kang, F.; Yang, C. Directing Lateral Growth of Lithium Dendrites in Micro-Compartmented Anode Arrays for Safe Lithium Metal Batteries. *Nat. Commun.* **2018**, *9*, 464. [[CrossRef](#)]
30. Han, X.; Gong, Y.; Fu, K.; He, X.; Hitz, G.T.; Dai, J.; Pearse, A.; Liu, B.; Wang, H.; Rubloff, G.; et al. Negating Interfacial Impedance in Garnet-Based Solid-State Li Metal Batteries. *Nat. Mater.* **2017**, *16*, 572–579. [[CrossRef](#)]
31. Luo, W.; Gong, Y.; Zhu, Y.; Li, Y.; Yao, Y.; Zhang, Y.; Fu, K.; Pastel, G.; Lin, C.-F.; Mo, Y.; et al. Reducing Interfacial Resistance between Garnet-Structured Solid-State Electrolyte and Li-Metal Anode by a Germanium Layer. *Adv. Mater.* **2017**, *29*, 1606042. [[CrossRef](#)]

32. Delaporte, N.; Guerfi, A.; Demers, H.; Lorrmann, H.; Paoella, A.; Zaghib, K. Facile Protection of Lithium Metal for All-Solid-State Batteries. *ChemistryOpen* **2019**, *8*, 192–195. [[CrossRef](#)]
33. Huang, C.-J.; Hsu, Y.-C.; Shitaw, K.N.; Siao, Y.-J.; Wu, S.-H.; Wang, C.-H.; Su, W.-N.; Hwang, B.J. Lithium Oxalate as a Lifespan Extender for Anode-Free Lithium Metal Batteries. *ACS Appl. Mater. Interfaces* **2022**, *14*, 26724–26732. [[CrossRef](#)]

Disclaimer/Publisher's Note: The statements, opinions and data contained in all publications are solely those of the individual author(s) and contributor(s) and not of MDPI and/or the editor(s). MDPI and/or the editor(s) disclaim responsibility for any injury to people or property resulting from any ideas, methods, instructions or products referred to in the content.